

General Disclaimer

One or more of the Following Statements may affect this Document

- This document has been reproduced from the best copy furnished by the organizational source. It is being released in the interest of making available as much information as possible.
- This document may contain data, which exceeds the sheet parameters. It was furnished in this condition by the organizational source and is the best copy available.
- This document may contain tone-on-tone or color graphs, charts and/or pictures, which have been reproduced in black and white.
- This document is paginated as submitted by the original source.
- Portions of this document are not fully legible due to the historical nature of some of the material. However, it is the best reproduction available from the original submission.

DRA- UNSIGNED
TITLE PAGE

NASA TECHNICAL MEMORANDUM

NASA TM X-64939



LIMIT CYCLE ANALYSIS OF LARGE SPACE TELESCOPE WITH CMG NONLINEARITY

(NASA-TM-X-64939) LIMIT CYCLE ANALYSIS OF
LARGE SPACE TELESCOPE WITH CMG NONLINEARITY
(NASA) 22 p HC \$3.25 CSCI 03A

N75-31965

G3/89 17986
Unclas

By S. M. Seltzer, B. C. Kuo,
and G. Singh
Systems Dynamics Laboratory

June 1975

NASA

*George C. Marshall Space Flight Center
Marshall Space Flight Center, Alabama*

1. REPORT NO. NASA TM X-64939		2. GOVERNMENT ACCESSION NO.		3. RECIPIENT'S CATALOG NO.	
4. TITLE AND SUBTITLE Limit Cycle Analysis of Large Space Telescope with CMG Nonlinearity				5. REPORT DATE June 1975	
				6. PERFORMING ORGANIZATION CODE	
7. AUTHOR(S) S. M. Seltzer, B. C. Kuo, and G. Singh				8. PERFORMING ORGANIZATION REPORT #	
9. PERFORMING ORGANIZATION NAME AND ADDRESS George C. Marshall Space Flight Center Marshall Space Flight Center, Alabama 35812				10. WORK UNIT, NO.	
				11. CONTRACT OR GRANT NO.	
				13. TYPE OF REPORT & PERIOD COVERED Technical Memorandum	
12. SPONSORING AGENCY NAME AND ADDRESS National Aeronautics and Space Administration Washington, D. C. 20546				14. SPONSORING AGENCY CODE	
15. SUPPLEMENTARY NOTES Presented as paper 74-874 at the AIAA "Mechanics and Control of Flight" Conference, Anaheim, California, August 5-9, 1974. Prepared by Systems Dynamics Laboratory.					
16. ABSTRACT The purpose of the investigation reported upon is to study the existence and characteristics of self-sustained oscillations in the dynamic behavior of the Large Space Telescope (LST) system due to the presence of nonlinear gimbal friction in the control moment gyroscopes (CMG's), if CMG's are selected for momentum exchange control. A continuous data single-axis model of the LST is considered. A solid friction model is used to represent CMG gimbal friction. A rigorous mathematical model is derived for use in a continuous describing function analysis. Conditions for self-sustained oscillations are then determined.					
17. KEY WORDS			18. DISTRIBUTION STATEMENT		
19. SECURITY CLASSIF. (of this report) Unclassified		20. SECURITY CLASSIF. (of this page) Unclassified		21. NO. OF PAGES 22	
				22. PRICE NTIS	

TABLE OF CONTENTS

	Page
I. INTRODUCTION	1
II. A SINGLE-AXIS MODEL OF THE LST CONTROL SYSTEM	2
III. MATHEMATICAL MODEL OF THE CMG FRICTIONAL NONLINEARITY	2
IV. A DESCRIBING FUNCTION FOR THE CMG GIMBAL FRICTION NONLINEARITY	6
V. STABILITY ANALYSIS BY USE OF THE DESCRIBING FUNCTIONS . .	10
VI. SIMULATION	11
VII. CONCLUSION	13
REFERENCES	16

LIMIT CYCLE ANALYSIS OF LARGE SPACE TELESCOPE WITH CMG NONLINEARITY

I. INTRODUCTION

The purpose of this investigation is to study the existence of self-sustained oscillations in the Large Space Telescope (LST) system due to the presence of nonlinear gimbal friction of the control moment gyroscope (CMG), if it is used as the momentum exchange controller for LST [1,2]. A continuous-data, single-axis model of the LST control system is considered with the CMG nonlinearity modeled as shown in Figure 1. One of the major differences seen in the various dynamic models of the CMG is in the accurate representation of the nonlinear friction characteristics of the CMG. The running friction of the gimbal axis consists of tachometer brush friction and the hysteresis drag which is associated with the brushless dc permanent-magnet torque motor. These frictional torques do not have significant effect on large motion gimbal-rate control loop performance, other than the power loss required to overcome the drag torque. However, the accurate representation of these torques for small motion has a pronounced influence on the gimbal-rate control loop small-motion performance. Whereas these effects have been second order for most previously reported systems, their effect is significant for the highly accurate performance requirements of LST. Therefore, the accurate modeling of these torques is essential in predicting the existence of limit cycles and the control loop response to very low level commands.

Using the solid friction model reported in Reference 3, a mathematical model of the CMG friction nonlinearity is derived for continuous describing function analysis. It is shown that the input-output characteristics of the nonlinearity are only a function of the

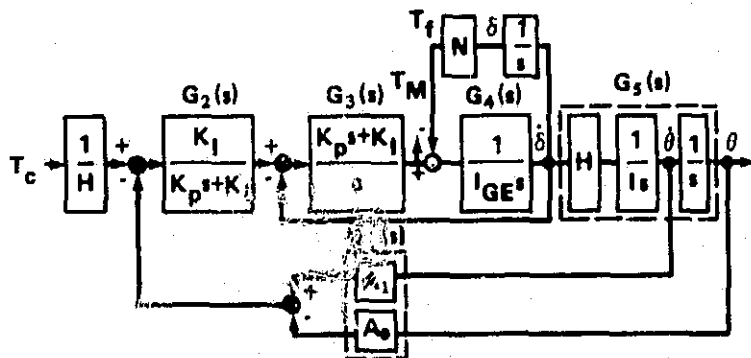


Figure 1. Single-axis model.

amplitude A of the input sinusoid and the nonlinearity parameters. A continuous describing function $N(A)$ is derived for the CMG nonlinearity, using the analytical frictional torque expression, and conditions for self-sustained oscillations are determined analytically. For the expected nominal values associated with CMG and LST parameter, an absence of limit cycle behavior is predicted. Digital computer simulations have been carried out to corroborate the analytical results.

II. A SINGLE-AXIS MODEL OF THE LST CONTROL SYSTEM

A simplified single-axis model of the LST fine-pointing control system is shown in Figure 1. The block diagram represents a simplified version of the LST control system obtained by neglecting the bending modes of the vehicle and the current loop and back emf of the CMG. However, the results of this report can be extended to more complex system models without difficulties.

The transfer function $G_5(s)$ denotes the vehicle dynamics of the LST as a single inertia I . The dynamics of the CMG are also modeled by a single inertia with the transfer function $G_4(s)$. The transfer functions $G_2(s)$ and $G_3(s)$ represent the CMG gimbal controller. The torsional feedback of the CMG output axis has been neglected. The block N denotes the CMG gimbal friction nonlinearity. The assumed characteristics of the nonlinearity are described and mathematically treated in the next section.

The controller for the LST vehicle is represented by the transfer function $G_1(s)$ which is of the proportional-plus-derivative (attitude-attitude rate) type. Since the objective of this report is not the design of the LST system, this conventional form of $G_1(s)$ is chosen for the purpose of computer simulation. It can be shown that the controller $G_1(s)$ is optimal in the sense of pole-placement design without the nonlinearity. Simulation results show that the system's response is quite satisfactory with this controller.

A list of symbols that describe the LST system variables and parameters, together with their numerical values, is given in Table 1.

III. MATHEMATICAL MODEL OF THE CMG FRICTIONAL NONLINEARITY

The running friction of the gimbal axis of the CMG consists of both the tachometer brush friction and the hysteresis drag, which is associated with the brushless dc permanent-magnet torque motor. These frictional torques do not have significant effect on large-motion gimbal-rate control loop performance other than through the power loss required to overcome the drag torque. In ordinary control system practice, these frictional characteristics can be either modeled as viscous or coulomb frictions or totally neglected if the amplitude of the frictional torque is relatively small. However, because of the fine-pointing accuracy and stability requirements of the LST system, accurate representation of the frictional torque becomes extremely important. For fine-pointing studies of the LST, the

TABLE 1. LST SYSTEM PARAMETERS

Variable	Description	Magnitude
H	CMG Angular Momentum	271 Nms
I	Vehicle Inertia	$1.354 \times 10^5 \text{ Nms}^2$
I_{GE}	Gimbal Inertia	5.0 Nms ²
K_I	Gimbal Rate Loop Integral Gain	$1.354 \times 10^4 \text{ Nm}$
K_p	Gimbal Rate Loop Gain	379 Nms
A_0	Vehicle Controller Coefficient	$2 \times 10^4 (\text{rad/s})^{-1}$
A_1	Vehicle Controller Coefficient	$3 \times 10^3 (\text{rad})^{-1}$
ϵ	Error Input Command to CMG	0.136 Nm
T_f	Torque Output of Nonlinearity	Nm
T_{f0}	Running Friction Torque	0.136 Nm
γ	Gimbal Bearing Parameter	$1.871 \times 10^5 (\text{Nms})^{-1}$
δ	Gimbal Position	rad
$\dot{\delta}$	Gimbal Velocity	rad/s
θ	Vehicle Position	rad
$\dot{\theta}$	Vehicle Velocity	rad/s

accurate modeling of the frictional torques is essential in predicting the existence of limit cycles and the control loop stability when the system is subject to very low-level disturbances and commands.

In this section, a mathematical model of the CMG friction nonlinearity is derived, based on the Dahl solid friction model [3,4]. The purpose of this model is that it can be used for the continuous-data describing function analysis of the nonlinear LST system.

A mathematical and simulation model of solid friction, such as that encountered in a bearing, was reported in Reference 4. Subsequent experimental studies have indicated that the frictional characteristics of the CMG can be approximated by this solid friction model. A more accurate model that has the same general characteristics as the one used herein has recently been developed [5]. However, since it is not precisely the same as that used in References 3 and 4, studies are now underway at NASA's Marshall Space Flight Center, by the co-authors of Reference 5, and other CMG developers, to develop an understanding of the effects of the more precise model on CMG and LST dynamics. If CMG output shaft friction torque versus shaft attitude (δ) or attitude rate ($\dot{\delta}$) were plotted, it could be seen that the simplified model used herein yields the envelope of the plots obtained with the model of Reference 5. Hence, it is felt (but as yet unproven) that the limit cycle predictions yielded by using the simplified model are approximately correct.

As indicated in References 3 and 4, the key to the simulation model is that the frictional torque, T_f , is a function of the CMG shaft displacement, δ , and can be differentiated with respect to time. Thus,

$$\frac{dT_f}{dt} = \frac{dT_f}{d\delta} \frac{d\delta}{dt} = T'_f \dot{\delta} \quad (1)$$

The frictional torque T_f can be generated by integrating both sides of equation (1) with respect to t .

In the simulation model, T'_f is generated by a function generator with input T_f . The output of the function generator is multiplied by $\dot{\delta}$ to give the right-hand side of equation (1), which is then integrated to yield T_f . Figure 2 is a simulation diagram of the CMG friction nonlinearity. The input of the model is $\dot{\delta}$, and the output is T_f . The relays are necessary because T_f is sensitive to the sign of $\dot{\delta}$.

It has been demonstrated experimentally that for solid rolling friction, the relation between T'_f and T_f may be approximated by a square-law expression,

$$T'_f \approx \gamma(T_f - T_{f_0})^2, \quad T_f \leq T_{f_0} = 0, \quad T_f > T_{f_0}; \quad (2)$$

where γ is a positive constant and T_{f_0} is the normalizing factor of T_f . However, the frictional torque is also velocity ($\dot{\delta}$) dependent, as shown in Figure 2. Therefore, equation (2) should be written

$$T'_f = \gamma(T_{f_i} - T_{f_0})^2 \quad (3)$$

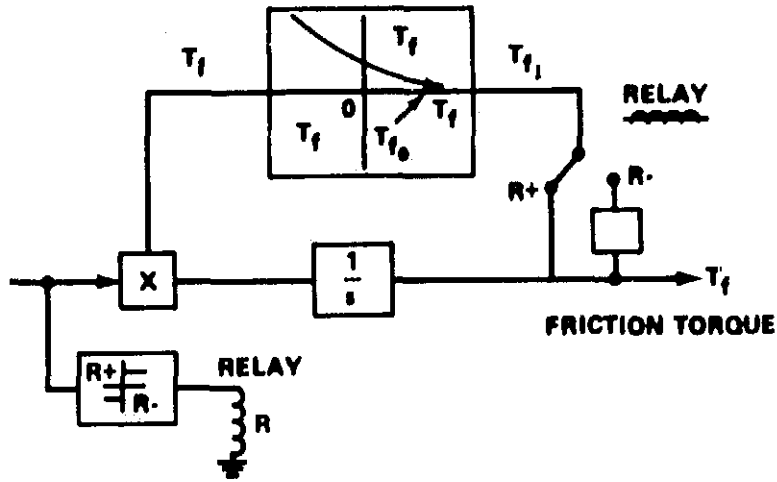


Figure 2. Simulation of CMG friction nonlinearity.

where

$$T_{f_i} = T_f \operatorname{sgn} \dot{\delta} \quad (4)$$

Integrating both sides of equation (2), one obtains

$$\delta + C = -\gamma (T_f^+ - T_{f_0})^{-1}, \quad \dot{\delta} \geq 0 \quad (5)$$

and

$$\delta - C = -\gamma (T_f^- - T_{f_0})^{-1}, \quad \dot{\delta} \leq 0 \quad ; \quad (6)$$

where C is the constant of integration and

$$\begin{aligned} T_f &= T_f^+, \quad \dot{\delta} \geq 0 \\ &= T_f^-, \quad \dot{\delta} \leq 0 \end{aligned} \quad (7)$$

If one assumes a sinusoidal input for δ , such as

$$\delta = A \cos \omega t \quad , \quad (8)$$

then

$$C = A + [\gamma(R+1) T_{f_0}]^{-1} \quad , \quad (9)$$

$$R \equiv -a^{-1} + \sqrt{(a^2 + 1)/a^2} \quad , \quad (10)$$

$$a \equiv 2\gamma A T_{f_0} \quad , \quad (11)$$

and solving equations (5) and (6) for T_f , one obtains

$$\begin{aligned} T_f &= T_f^+ = -[\gamma(A \cos \omega t + C)]^{-1} + T_{f_0} \quad , \quad \dot{\delta} \geq 0 \\ &= T_f^- = -[\gamma(A \cos \omega t - C)]^{-1} - T_{f_0} \quad , \quad \dot{\delta} \leq 0 \end{aligned} \quad (12)$$

IV. A DESCRIBING FUNCTION FOR THE CMG GIMBAL FRICTION NONLINEARITY

In order to derive a describing function for the assumed CMG nonlinearity, one assumes a sinusoidal input to the nonlinearity of the form of equation (8). The output of the nonlinearity, T_f , is approximated by the fundamental component of its Fourier series. Since the input-output relation of the nonlinearity is symmetrical about the zero-torque axis, there is no dc component in the series. Thus,

$$T_f \approx T_1(t) = \bar{A}_1 \sin \omega t + \bar{B}_1 \cos \omega t \quad , \quad (13)$$

where

$$\bar{A}_1 = \frac{1}{\pi} \int_0^{2\pi} T_f \sin \omega t d\omega t = \frac{1}{\pi} \int_0^{\pi} T_f^- \sin \omega t d\omega t + \frac{1}{\pi} \int_{\pi}^{2\pi} T_f^+ \sin \omega t d\omega t \quad (14)$$

and

$$\begin{aligned}\bar{B}_1 &= \frac{1}{\pi} \int_0^{2\pi} T_f \cos \omega t \, d\omega t = \frac{1}{\pi} \int_0^{2\pi} T_f^- \cos \omega t \, d\omega t \\ &+ \frac{1}{\pi} \int_{\pi}^{2\pi} T_f^+ \cos \omega t \, d\omega t \quad .\end{aligned}\quad (15)$$

Equation (13) can also be written as

$$T_1(t) = \sqrt{\bar{A}_1^2 + \bar{B}_1^2} \cos(\omega t - \phi) \quad , \quad (16)$$

where

$$\phi = \tan^{-1} (\bar{A}_1 / \bar{B}_1) \quad , \quad (17)$$

or in phasor notation,

$$T_1(i\omega) = \sqrt{\bar{A}_1^2 + \bar{B}_1^2} \exp [i \tan^{-1} (\bar{A}_1 / \bar{B}_1)] \quad . \quad (18)$$

The describing function is given by

$$N(A) = T_1(i\omega) / \delta(i\omega) = (\bar{B}_1 / A) - i(\bar{A}_1 / A) = N_1 + iN_2 \quad . \quad (19)$$

The coefficients \bar{A}_1 and \bar{B}_1 can be obtained by substituting equation (12) into equations (14) and (15), respectively, and performing the appropriate integrations. The results are:

$$\begin{aligned}\bar{A}_1 &= -(4T_{f_0} / \pi) + 2\ln[(C + A) / (C - A)] / \pi A \gamma \\ &= (2T_{f_0} / \pi a) [\ln(a + \sqrt{a^2 + 1})^2 - 2a]\end{aligned}\quad (20)$$

and

$$\bar{B}_1 = 2[(C/\sqrt{C^2 - A^2}) - 1]/\gamma A$$

$$= (4T_{f_0}/a) \sqrt{[a^2 + a + 1 + (a + 1)\sqrt{a^2 + 1}]/2(a + \sqrt{a^2 + 1}) - 1} \quad (21)$$

For stability analysis, it is of interest to determine the behavior of $-1/N(A)$. This may be computed readily by use of equations (19) through (21). Figure 3 shows the magnitude (db) versus phase (degrees) plots of $-1/N(A)$ for $\gamma = 1.871 \times 10^5$, 1.871×10^6 , and 1.87×10^7 (Nms) $^{-1}$, as the magnitude of A varies.

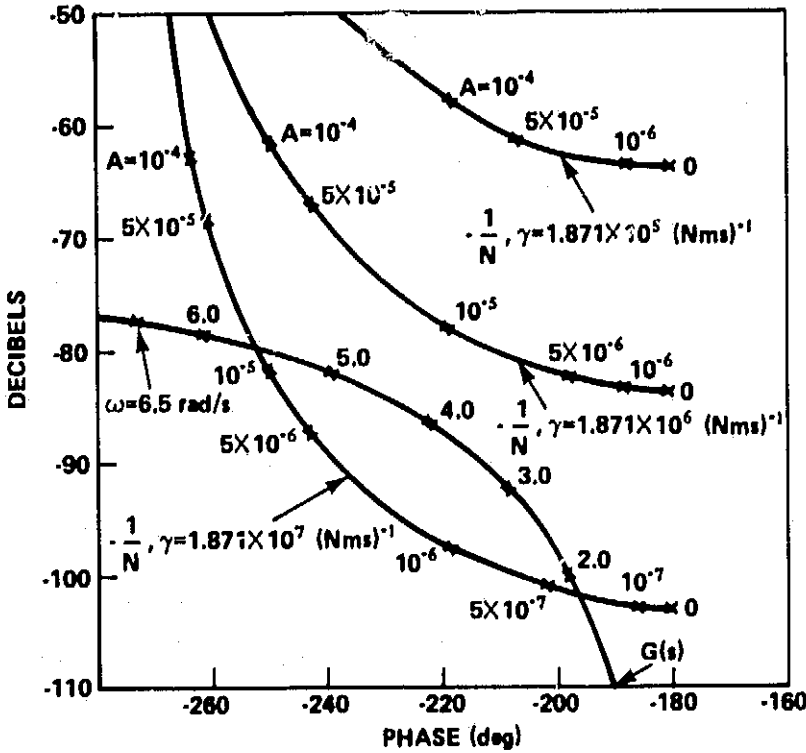


Figure 3. Plots of $-1/N$ and $G(S)$.

Figure 3 shows that as A approaches zero, the magnitude of $-1/N(A)$ in db approaches $20 \log_{10} [1/\gamma T_{f_0}]$ and the phase is -180 degrees. This asymptotic behavior of $-1/N(A)$ for small values of A may be derived analytically by expanding the logarithmic term in equation (20) and using relations (7) through (9):

$$\lim_{A \rightarrow 0} (\bar{A}_1/A) = 0 \quad . \quad (22)$$

Similarly, by expanding the square root term of equation (21) into a power series one obtains

$$\lim_{A \rightarrow 0} (\bar{B}_1/A) = \sigma \quad , \quad (23)$$

where

$$\sigma \equiv \gamma T_{f_0}^2 \quad . \quad (24)$$

Thus,

$$\lim_{A \rightarrow 0} [-1/N(A)] = \lim_{A \rightarrow 0} \{ -[(\bar{B}_1/A) - i(\bar{A}_1/A)] \}^{-1} = -1/\sigma \quad . \quad (25)$$

For large values of A , the value of C becomes

$$\lim_{A \rightarrow \infty} C = \lim_{A \rightarrow \infty} (A + 2/\gamma T_{f_0}) = \lim_{A \rightarrow \infty} [A] \rightarrow \infty \quad . \quad (26)$$

Then,

$$\lim_{A \rightarrow \infty} (\bar{A}_1/A) = \lim_{A \rightarrow \infty} (-4T_{f_0}/\pi A) = -0 \quad , \quad (27)$$

and

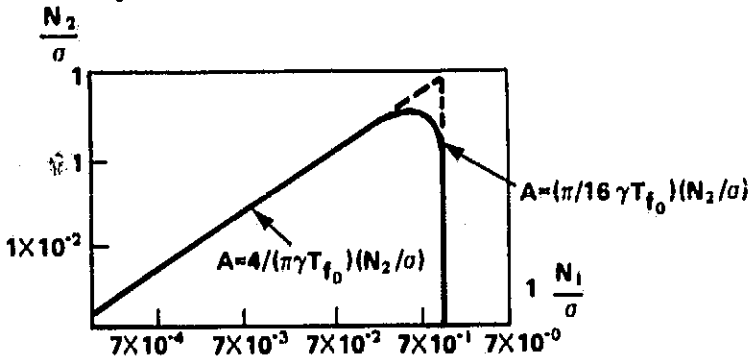
$$\lim_{A \rightarrow \infty} (\bar{B}_1/A) = +0 \quad . \quad (28)$$

Thus,

$$\lim_{A \rightarrow \infty} [-1/N(A)] = -1/0 = \infty/-270^\circ \quad (29)$$

As shown in Figure 3, the gain-phase plots of $-1/N(A)$ approach $\infty/-278^\circ$ as $A \rightarrow \infty$ for all values of γ and T_{f_0} .

Alternately, a general map of N_2 versus N_1 (as a function of the argument A) may be developed for use in this and future limit cycle investigations for this particular form of nonlinearity (Fig. 4) [6]. It is universal in the sense that it permits one to choose any design values for T_{f_0} and γ , and see their effect on the N_2 versus N_1 map.



NOTE: DESCRIBING FUNCTION ASYMPTOTES:
VALUES FOR A ARE FOUND FOR CURVE
CURVES NO. 1 & NO. 2, RESPECTIVELY.
BY READING THE VALUE OF N_2/a FOR THE
POINT IN QUESTION AND THEN APPLYING
THE APPROXIMATION INDICATED.

Figure 4. Normalized Dahl describing function locus.

V. STABILITY ANALYSIS BY USE OF THE DESCRIBING FUNCTION

The system described in Figure 1 appears to be suitable for describing function analysis because it is low-pass and the system parameters are assumed time-invariant. The condition for a self-sustained oscillation in a linear system with a nonlinearity is given by

$$1 + N(A) G(i\omega) = 0 \quad (30)$$

where $N(A)$ is the describing function of the nonlinearity and $G(i\omega)$ is the transfer function of the system which is seen by the nonlinearity. The solution of equation (30) can be obtained graphically by plotting the $G(i\omega)$ curve for the system and the $-1/N(A)$ curve for the nonlinearity. The point of intersection of these curves will yield the solution to equation (30). The magnitude and frequency of the oscillation corresponds to the values of A and ω at the solution point.

For the LST system in Figure 1, the transfer function which the nonlinear element sees is

$$G(s) = \frac{Is^2}{IIGEs^4 + IKps^3 + IKIs^2 + k_IHA_1s + K_IHA_0} \quad (31)$$

The relevant portions of the frequency-domain plot of $G(s)$ are super-imposed on the $-1/N$ curves of Figure 3 in db versus phase coordinates. With $\gamma = 1.87 \times 10^7$, the $-1/N$ curve intersects the $G(s)$ curve at two points. The stable point for sustained oscillations is the one on the left at the higher frequency. The approximate magnitudes for frequencies of the oscillations are 3×10^{-7} rad and 1.8 rad/s, respectively, for the unstable limit cycle, and 2×10^{-5} rad and 5.6 rad/s, respectively, for the stable limit cycle. The curves in Figure 3 also show that for γ considerably smaller than 1.871×10^7 , the system will exhibit a stable response.

Following the alternate approach begun in the previous section, limit cycle conditions and characteristics may be predicted, using the parameter plane technique [6]. Specifically, one may place the describing function locus (Fig. 4) on an N_1, N_2 parameter plane stability map to analyze and predict limit cycle behavior. The result is portrayed on Figure 5 and agrees with the stability analysis technique portrayed on Figure 3.

VI. SIMULATION

To corroborate these results, the LST system was simulated on a digital computer. The CMG friction nonlinearity was simulated as shown in Figure 2. For the computer simulation, the input to the LST system, T_c , was set to zero, along with all of the initial states, except for the vehicle position, θ , which was set at 5×10^{-5} rad. This value was chosen so that the input signal to the nonlinearity, δ , would be large enough to cause the torque to saturate but not so large as to exceed the limiting value of the input signal. The quantities plotted from the simulation runs are vehicle attitude and attitude rate, θ and $\dot{\theta}$, and friction torque, T_f .

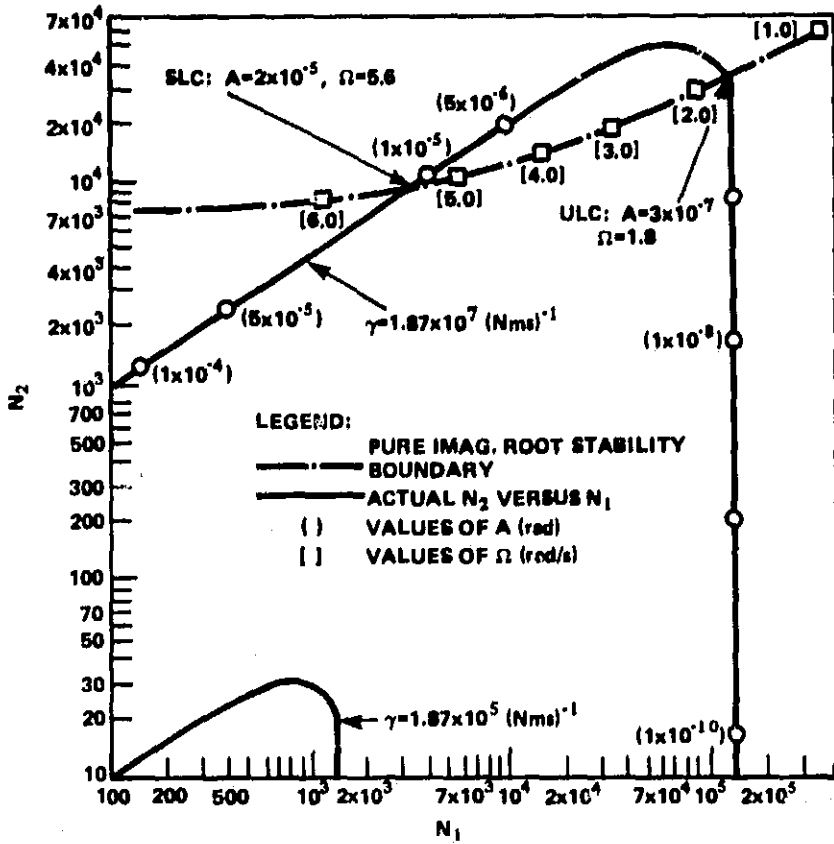


Figure 5. N_1 - N_2 parameter plane.

Figure 6 shows the plots with $\gamma = 1.871 \times 10^7$. It is observed from the plot of T_f in Figure 6 that the system has a sustained oscillation. This oscillation is not seen on the other plots because of the large initial transients. For this reason, the vertical scale of the plot is adjusted (Fig. 7) to show the oscillations. The frequencies and magnitudes of oscillations obtained are quite close to the predicted values. The small discrepancy is partly attributed to the quantization caused by the nonlinearity implementation on the digital computer.

Figure 8 shows the response plots with $\gamma = 1.871 \times 10^5$. As predicted, the system is stable for the lower values of γ .

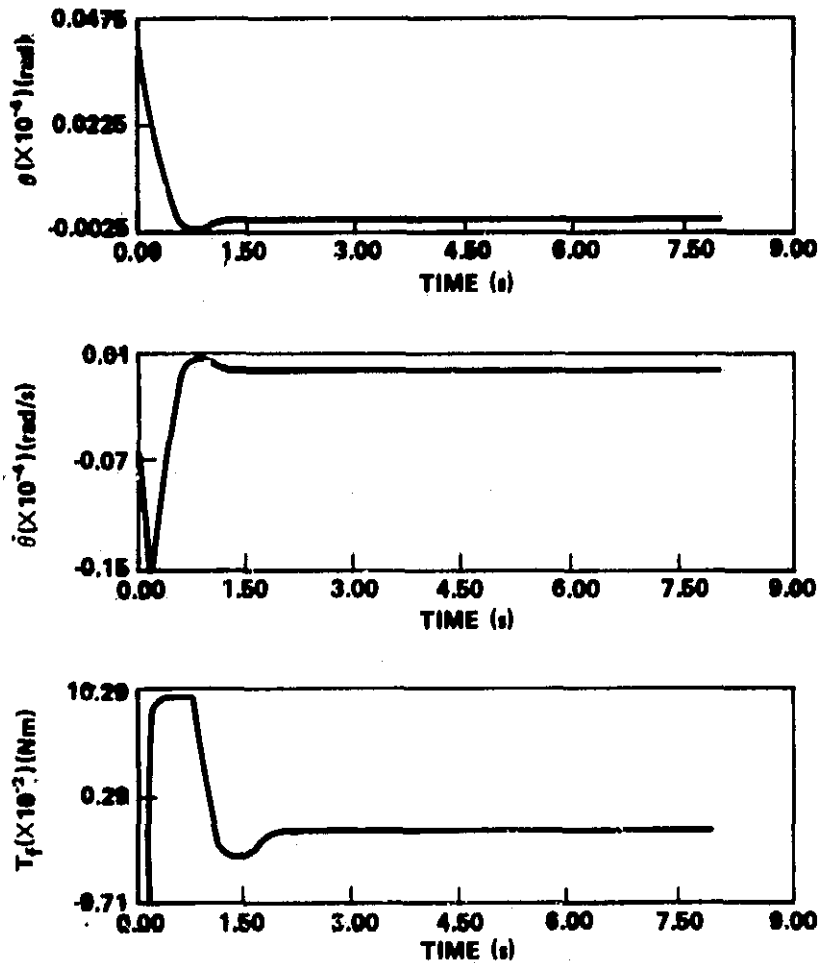


Figure 6. Simulation ($\gamma = 1.871 \times 10^7$).

VII. CONCLUSION

For numerical values considered to be representative of the LST and CMG's (if they are used), analysis of the simplified continuous-data model with a solid friction CMG nonlinear characteristic indicates (and analogue simulation confirms) the absence of limit cycle behavior due to the CMG nonlinearity. It must be borne in mind that the analysis has not yet included the dynamic effects induced by the sampling phenomena of the onboard digital computer. Experience with past spacecraft would lead one to expect quantization, for example, to induce limit cycling of the plant.

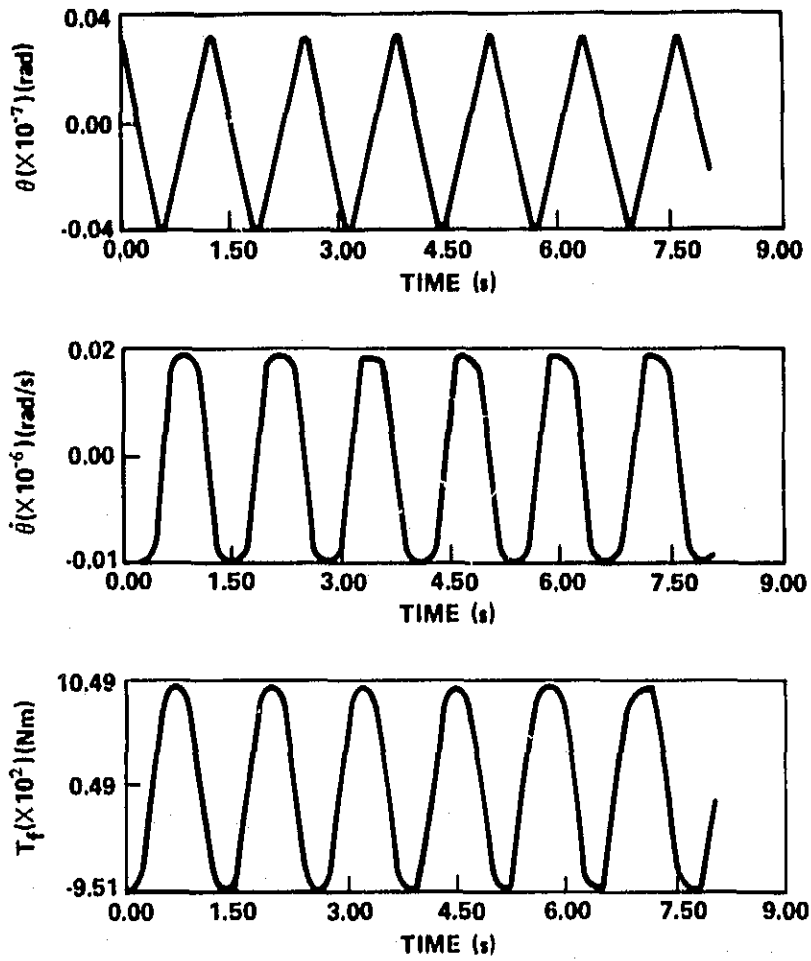


Figure 7. Simulation ($\gamma = 1.871 \times 10^7$): steady state.

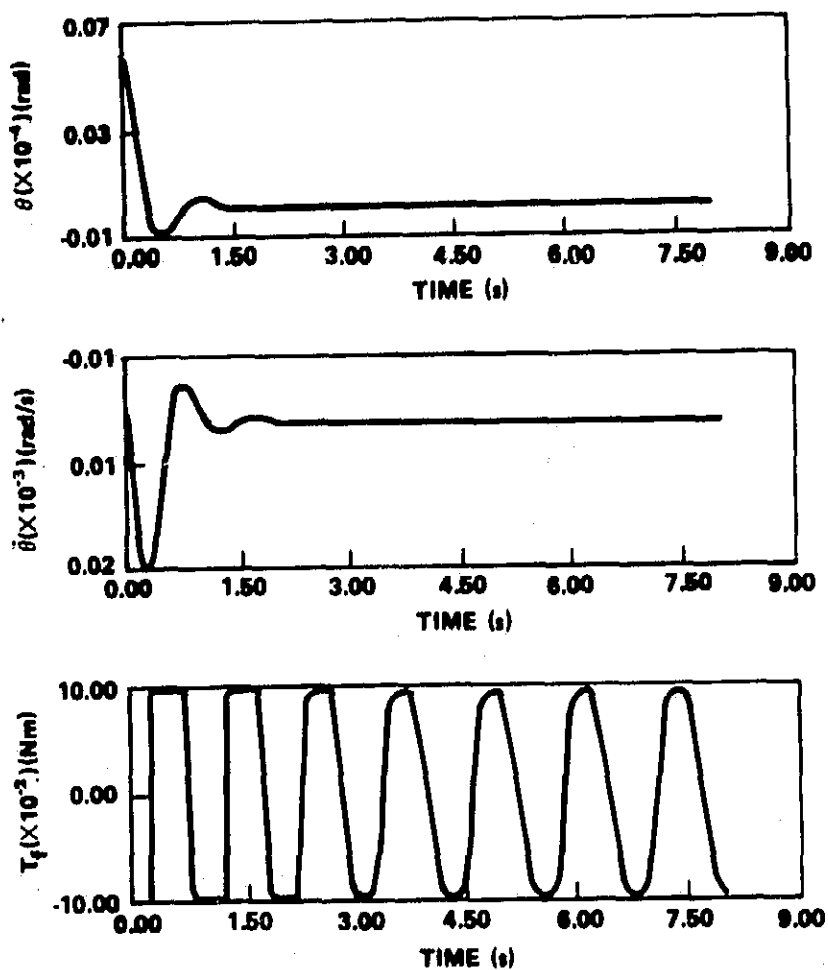


Figure 8. Simulation ($\gamma = 1.871 \times 10^5$).

REFERENCES

1. O'Dell, C. R.: Optical Space Astronomy and Goals of the Large Space Telescope. Astronautics & Aeronautics, Vol. II, No. 4, April 1973, pp. 22-27.
2. Proise, M.: Fine Pointing Performance Characteristics of the Orbiting Astronomical Observatory (OAO-3). Presented at the AIAA Guidance and Control Conference, Paper No. 73-158, Key Biscayne, Florida, August 20-22, 1973.
3. Dahl, P. R.: A Solid Friction Model. TOR-158 (3107-18), The Aerospace Corporation, El Segundo, California, May 1968.
4. Nurre, G. S.: An Analysis of the Dahl Friction Model and Its Effect on a CMG Gimbal Rate Controller. NASA TM X-64934, June 1975.
5. Rittenhouse, D. L. and Osborne, N. A.: Modeling of Friction and Its Effects on Fine Pointing Control. Presented at the AIAA Mechanics and Control of Flight Conference, Paper No. 74-875, Anaheim, California, August 5-9, 1974.
6. Seltzer, S. M.: CMG-Induced LST Dynamics. NASA TM X-64833, February 1974.

APPROVAL

LIMIT CYCLE ANALYSIS OF LARGE SPACE TELESCOPE WITH CMG NONLINEARITY

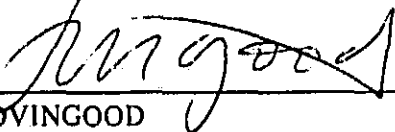
By S. M. Seltzer, B. C. Kuo, and G. Singh

The information in this report has been reviewed for security classification. Review of any information concerning Department of Defense or Atomic Energy Commission programs has been made by the MSFC Security Classification Officer. This report, in its entirety, has been determined to be unclassified.

This document has also been reviewed and approved for technical accuracy.



JAMES C. BLAIR,
Chief, Control Systems Division



J. A. LOVINGOOD
Director, Systems Dynamics Laboratory